Research Article | Open Access

Microstructures

Chen et al. Microstructures 2026, 6, 2026070 DOI:10.20517/microstructures.2025.91

Entropy engineering in ferroelectric/dielectric superlattices for ultrahigh-efficiency superparaelectrics energy storage capacitors

Qianxin Chen[1,2], Mingqiang Cheng[3], Peipei Su[4], Jinbin Wang[1], Xiangli Zhong[1], Hongjia Song[1], Jiangyu Li[3], Gaokuo Zhong[2]

Keywords:
Energy storage, superlattice, entropy engineering, superparaelectrics, ferroelectric film

Citation: Chen, Q.; Cheng, M.; Su, P.; Wang, J.; Zhong, X.; Song, H.; Li, J.; Zhong, G. Entropy engineering in ferroelectric/dielectric superlattices for ultrahigh-efficiency superparaelectrics energy storage capacitors. *Microstructures* **2026**, *6*, 2026070. https://dx.doi.org/10.20517/microstructures.2025.91

Received: 24 Jun 2025 **First Decision:** 27 Aug 2025 **Revised:** 8 Sep 2025 **Accepted:** 30 Sep 2025 **Published:** 27 May 2026

Academic Editor: Zibin Chen
Copy Editor: Ting-Ting Hu
Production Editor: Ting-Ting Hu

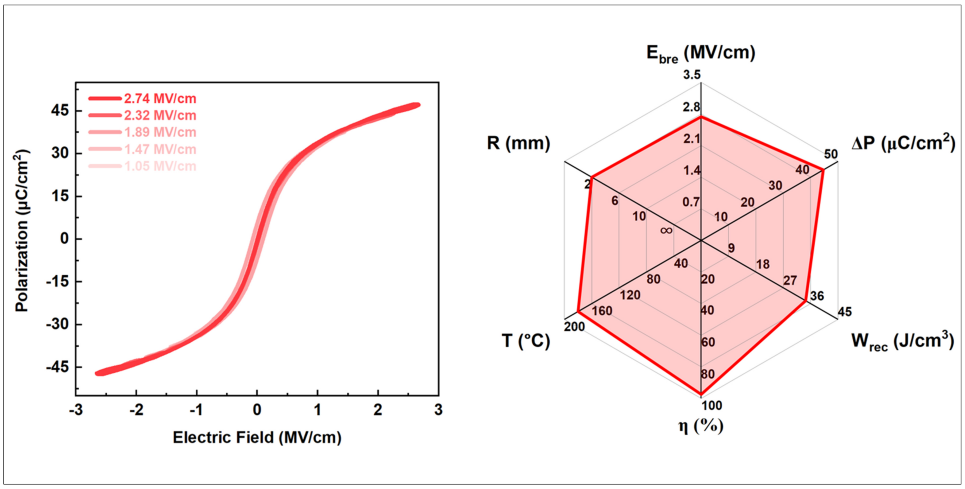

Abstract

Thin-film capacitors exhibit significant application potential owing to their rapid charge/discharge characteristics and high-power density. Individual engineering strategies can effectively enhance either breakdown strength (E_{bre}) or polarization difference to improve energy storage performance. However, such enhancement typically leads to unilateral optimization of either energy density (W_{rec}) or energy efficiency (η) and fails to achieve an optimal trade-off between these, resulting in limitation fundamentally constrains the simultaneous enhancement. In this work, we propose multi-level synergistic modulation strategy, realizing synchronous optimization of multiple parameters to achieve breakthrough in comprehensive energy storage performance. Taking classic $BaTiO_3$ ferroelectric as example, we implemented interface engineering strategy to simultaneously enhance the E_{bre} and reduce remnant polarization. Combined with entropy optimization strategy, this approach further increased the E_{bre} while significantly boosting saturation

[1]National-Provincial Laboratory of Special Function Thin Film Materials, School of Materials Science and Engineering, Xiangtan University, Xiangtan 411105, Hunan, China.
[2]Changsha Semiconductor Technology and Application Innovation Research Institute, College of Semiconductors (College of Integrated Circuits), Hunan University, Changsha, Hunan, China.
[3]Department of Materials Science and Engineering, Southern University of Science and Technology, Shenzhen 518055, Guangdong, China.
[4]Shenzhen Institutes of Advanced Technology, Chinese Academy of Sciences, Shenzhen 518055, Guangdong, China.

Correspondence to: Prof. Xiangli Zhong, National-Provincial Laboratory of Special Function Thin Film Materials, School of Materials Science and Engineering, Xiangtan University, Xiangtan 411105, Hunan, China. E-mail: xlzhong@xtu.edu.cn; Prof. Gaokuo Zhong, Changsha Semiconductor Technology and Application Innovation Research Institute, College of Semiconductors (College of Integrated Circuits), Hunan University, Changsha, Hunan, China. E-mail: gkzhong@hnu.edu.cn

polarization. The developed $BaTiO_3/SrTiO_3$-$BiFeO_3$ superparaelectric film capacitor demonstrate exceptional energy storage performance, achieving ultrahigh η of 97.35% and high W_{rec} of 40.60 J/cm^3, increasing to 133.56% and 492.72% comparing to the pure film. Moreover, the same system on flexible substrates shows comparable outstanding energy storage performance, with excellent operational stability across wide temperatures and under mechanical deformation. These results confirm the universality of strategy and pave the way for multifunctional flexible capacitors.

INTRODUCTION

High-performance capacitors are critically application potential in pulsed power systems, hybrid electric vehicles, and advanced renewable energy storage due to their rapid charge-discharge capability and high-power density[1-4]. For capacitors, energy density (W_{rec}) and energy efficiency (η) serve as critical metrics for evaluating their energy storage performance, reflecting the amount of energy that can be stored per unit volume[5]. Higher W_{rec} and η indicate that the capacitor can store energy more efficiently within a limited volume and release more energy during charge-discharge cycles[5]. Typically, the W_{rec} and η are quantitatively calculated through the following formulas[6]: $W_{rec} = \int_{P_r}^{P_s} E_{bre} dP$ and $\eta = W_{rec}/W_{rec} + W_{loss}$, where P_s, P_r, breakdown strength (E_{bre}) and W_{loss} represent saturation polarization, remnant polarization, E_{bre}, and energy loss density, respectively. Thus, enhancing E_{bre} and maximizing the ΔP (The difference between P_s and P_r) are effective strategies for achieving superior capacitor performance[7,8]. Among various dielectric film materials for capacitive energy storage, ferroelectric (FE) materials have proven to be one of the most promising candidates for high-performance capacitors due to their high E_{bre}, large saturation polarization, and excellent fatigue resistance[9-12]. Although the large P_r caused by hysteretic switching of large FE domains, results in low η, presenting a major challenge for enhancing energy storage performance[13,14]. Recent advances in interface engineering [such as integrating dielectric interlayers into FE films to construct multilayer or superlattice structure (SLs)] demonstrate improved ΔP and E_{bre}, thereby boosting η[15-20]. In particular, capacitors incorporating linear dielectric $SrTiO_3$ (STO) with ultrahigh E_{bre} and η, showing the most pronounced reduction in P_r, as demonstrated in systems like $BaTiO_3$ (BTO)[16], $BiFeO_3$ (BFO)[17], $Bi_{3.15}Nd_{0.85}Ti_3O_{12}$ (BNT)[18], and (Pb, La)(Zr, Ti)O_3 (PLZT)[19,20]. Nevertheless, the non-polar characteristic of STO fundamentally precludes any enhancement of P_s and makes it impossible to increase the W_{rec} in capacitors, meaning individual engineering strategies exhibit inherent limitations in achieving a balanced improvement in both W_{rec} and η. Therefore, a holistic strategy that synergistically optimizes multiple parameters is critically needed to achieve breakthroughs in comprehensive energy storage performance.

Researchers have employed composite engineering, multi-scale engineering, and combinatorial engineering, to effectively modulate the composition, microstructure, and local structure of dielectric materials[21-23]. These approaches enable precise control over key properties such as E_{bre}, P_s, P_r and thermal stability, demonstrating excellent tunability, versatility, and practicality[24-26]. Liu *et al*. achieved a reduced hysteresis and significantly enhanced E_{bre} in $(Pb_{0.875}La_{0.05}Sr_{0.05})(Zr_{0.695}Ti_{0.005}Sn_{0.3})O_3$ multilayer ceramic capacitors through a combined compositional and structural optimization strategy, realizing an impressive ultrahigh W_{rec} with high η[24]. Meanwhile, Ma *et al*. proposed a synergistic nano-micro engineering approach that not only improved the microstructural homogeneity of FE multilayer ceramics but also facilitated the transformation of FE domains into polar nanodomains, thereby enhancing relaxor behavior and energy storage performance[25]. For interface engineering primarily based on STO, the entropy optimization strategy is undoubtedly the most suitable synergistic approach. By incorporating multiple principal elements to form a configuration-entropy system, it simultaneously achieves grain refinement and enhanced relaxor behavior[27-33]. This strategy not only compensates for the inability of STO to improve P_s but also significantly increases the E_{bre}, thereby synergistically enhancing both W_{rec} and η, which ultimately expected to achieve comprehensive energy storage performance enhancement. In this study, we proposed a multi-level synergistic modulation strategy

involving interface engineering and entropy optimization, which enables effective multi-directional regulation to simultaneously enhance energy storage density and efficiency. Taking BTO as a model system, we designed and fabricated a BTO/STO-BFO superparaelectric (SPE) film capacitor by introducing STO interlayers and BFO solid-solution. The multiscale structural modulation substantially enhanced E_{bre} and P_s with reducing P_r, reaching an ultra-high η of 97.35% and a high W_{rec} of 40.60 J/cm^3, which represents improvements of 133.56% and 492.72% comparing to the pure BTO film. Remarkably, the flexible capacitors base on same strategy exhibits excellent energy storage performance and stability under harsh thermal and mechanical bending conditions, establishing a promising platform for developing flexible capacitors with high energy storage capacity.

MATERIALS AND METHODS

Sample Fabrication: The (111)-STO substrate and the flexible mica substrate thinned mechanically were placed into pulsed laser deposition system (HT-PLD, RP-HT-102 purchased from Shenzhen Arrayed Materials Co., Ltd. in China) for the following thin films growth, to construct BTO-based capacitors (including BTO, BTO/STO and BTO/STO-BFO). In pulsed laser deposition (PLD) chamber in BTO-based capacitors on (111)-STO substrate, the bottom electrode layer of $SrRuO_3$ (SRO) was first grown on (111)-STO substrate using a KrF excimer laser (λ = 248 nm, Coherent) operated at 690 °C and 80 mTorr oxygen pressure. Then, through the rapid switching mode of multi-target by PLD, the alternating stacks of BTO and STO layers and the solid-solution of BFO were deposited under an oxygen pressure of 5 mTorr at 690 °C. During the deposition process, the fixed total excitation number was 15,000, and the cycle period was 50 times. Among them, the excitation number ratio of BTO, STO and BFO was 12:2:1. For flexible BTO-based capacitors, to weaken the van der Waals forces on the surface of the mica substrate, a CFO ($CoFe_2O_4$) film was deposited as a buffer layer before the bottom electrode layer SRO, with an oxygen pressure of 50 mTorr and 600 °C. The CFO, SRO and BTO/STO-BFO layers were grown at a pulse repetition rate of 10 Hz under laser energy of 330, 370 and 350 mJ, respectively. To construct the capacitor structure, a small ion sputterer (SBC-12, purchased from Beijing KYKY Co., Ltd. in China) was used to deposit a circular Au top electrode with a diameter of 100 μm. The detailed growth parameters and the design of the functional layer structure are provided in Supplementary Tables 1 and 2.

Characterization and electrical Properties: The crystalline structure of the BTO-based capacitors were characterized by using XRD (Bruker/AXS D8-ADVANCE ECO diffractometer). The reciprocal space mapping (RSM) data were performed via Rigaku Smartlab diffractometer. The cross-sectional sectional transmission electron microscopy (STEM) specimens were lift-out by Focused Ion beam (FIB, Thermal Fisher Helios G4). STEM images were obtained through an aberration-corrected JEM-ARM300FS equipped with Energy-dispersive X-ray spectroscopy (EDS) detectors. The P-E hysteresis loops and I-E curves were measured using a Radiant Technology Precision Premium II tester (Radiant Technologies, Inc.) at a frequency of 10 kHz. For the bending test, the mold with different bending radii were used to adhere sample on its surface, and the bending performances of sample were tested.

RESULTS AND DISCUSSION

The schematic diagram of our ideal design concept is illustrated in Figure 1A-C. By employing a multi-level synergistic modulation strategy involving interface engineering and entropy optimization, we achieve a transition from FE to relaxor ferroelectric (RFE), ultimately reaching a SPE state. In conventional FE oxides, the domain structure typically exhibits long-range order with large grain sizes, making a relatively large polarization intensity in macroscopic properties [Figure 1A]. While this leads to large hysteresis, small W_{rec}, and low η, which limit their practical applications in energy storage[7]. Typically, introducing a linear dielectric material with high η and E_{bre} as a blocking layer to form a FE/dielectric SLs. This approach can

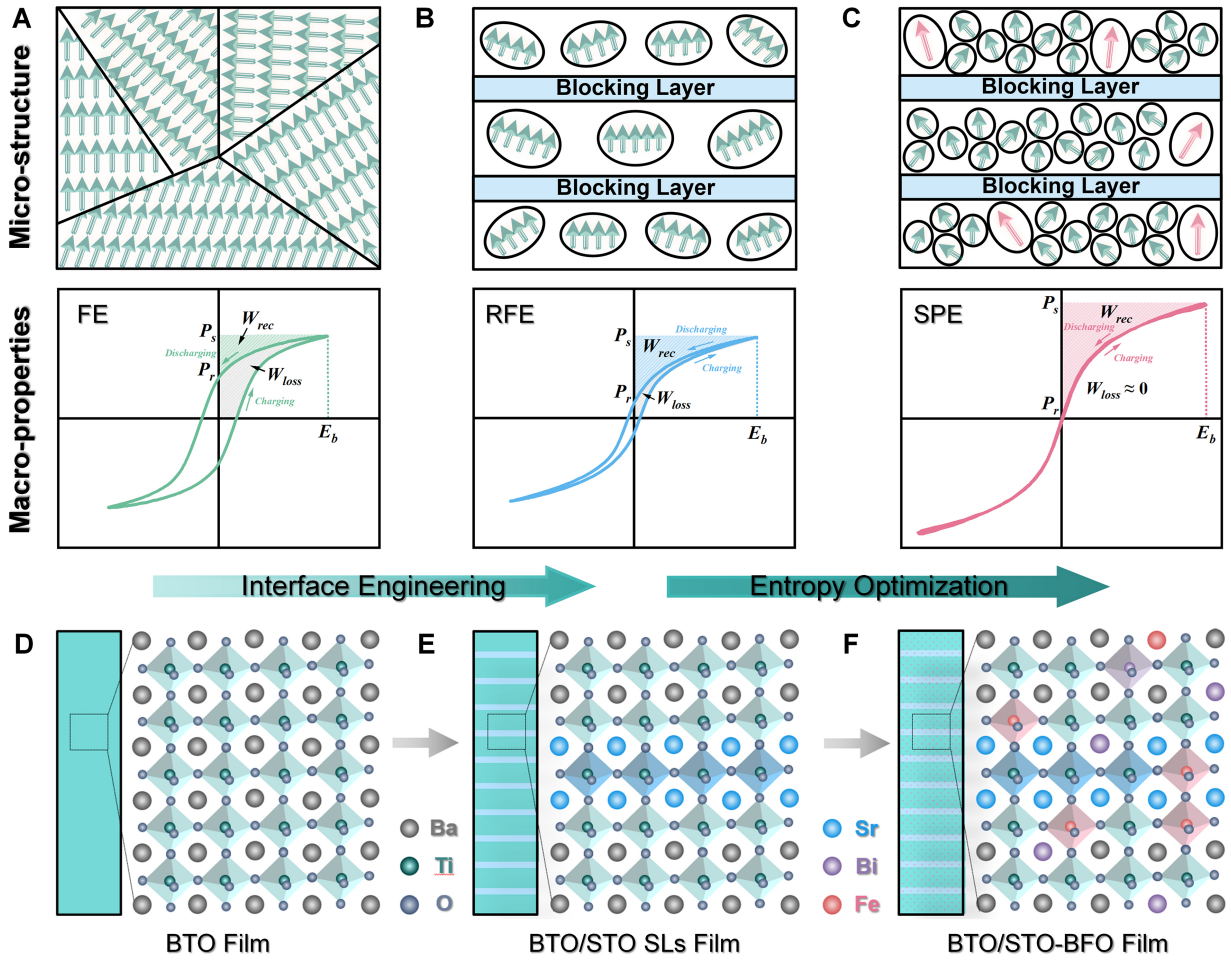

Figure 1. Design concept and preparation of SPE film capacitor. (A-C) Micro-structure and macro-property of (A) FE, (B) RFE and (C) SPE by interface engineering and entropy optimization; (D-F) Schematic diagram of crystal structure for (D) BTO, (E) BTO/STO SLs and (F) BTO/STO-BFO SPE films. FE: Ferroelectric; RFE: relaxor ferroelectric; SPE: superparaelectric; BTO: barium titanate; STO: strontium titanate; BFO: bismuth ferrite; SLs: superlattices; P_s: saturation polarization; P_r: remanent polarization; E_b: electric breakdown strength; W_{rec}: recoverable energy density; W_{loss}: energy loss.

effectively disrupt long-range FE ordering and reduce grain size [Figure 1B], thereby diminishing P_r and hysteresis while enhancing the E_{bre}, resulting in increasing the W_{rec} and η. Nevertheless, the limited P_s and the existing hysteresis remain challenges. To overcome these limitations, we further integrate an entropy optimization strategy with the FE/dielectric SLs. This methodology enables simultaneous grain size refinement and enhancement of local polarization intensity, facilitating the transition from RFE to SPE and increasing comprehensive energy storage performance of the capacitor in Figure 1C. The developed dielectric capacitor shows great potential for next-generation energy storage applications, offering simultaneous achievement of ultra-high η and outstanding W_{rec}. To validate our design strategy, we selected the well-established BTO FE system [Figure 1D]. By utilizing STO, a linear dielectric with a compatible crystal structure and lattice matching, we constructed BTO/STO SLs [Figure 1E] to enhance the E_{bre} and η. We have previously established the efficacy of this strategy through systematic studies of BNT-STO and PLZT-STO system[18,20]. Furthermore, we incorporated a solid-solution BFO FE with known for high polarization intensity into the BTO/STO SLs [Figure 1F] to simultaneously boost both the P_s and E_{bre}, achieving significant improvement in energy storage performance. Using PLD with a multi-target rapid switching, we epitaxially grew BTO, BTO/STO SLs, and BTO/STO-BFO SPE films on (111)-oriented STO/SRO substrates, and the Au top electrodes were sputtered to construct capacitors. Additional experimental details can be found in the MATERIALS AND METHODS.

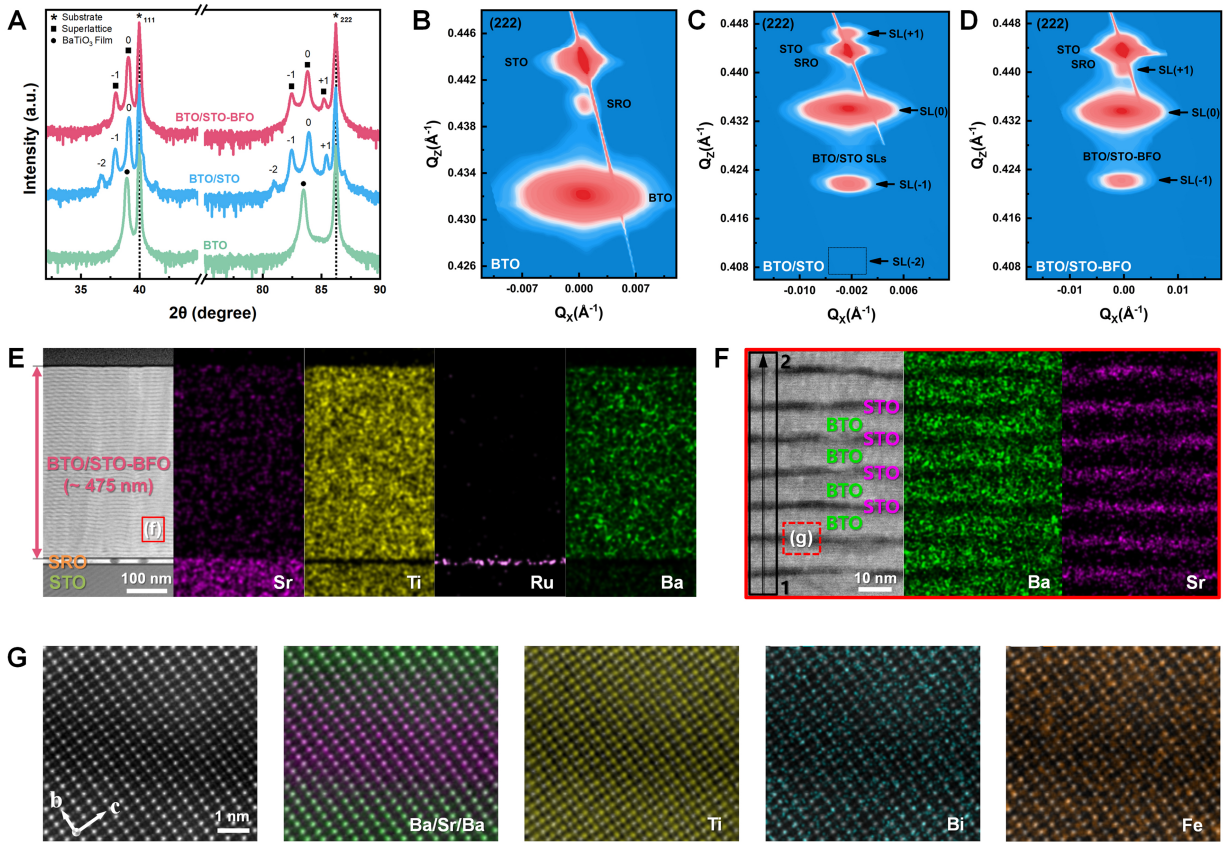

Figure 2. The microstructure of BTO/STO-BFO SPE film on (111)-STO substrate. (A) The XRD of BTO, BTO/STO SLs and BTO/STO-BFO SPE films; (B-D) The RSM of (B) BTO, (C) BTO/STO SLs and (D) BTO/STO-BFO SPE films around the (222) reflections; (E) The STEM image and EDS of the BTO/STO-BFO SPE film; (F) The STEM image of BTO/STO SLs with the corresponding EDS element mapping; (G) The high-resolution STEM image of BTO/STO-BFO SPE film with the corresponding EDS element mapping. BTO: Barium titanate; STO: strontium titanate; BFO: bismuth ferrite; SLs: superlattices; SPE: superparaelectric; XRD: X-ray diffraction; RSM: reciprocal space mapping; STEM: scanning transmission electron microscopy; EDS: energy-dispersive X-ray spectroscopy.

The X-ray diffraction pattern (XRD) of the BTO films is presented in Figure 2A, where (iii) reflections from BTO (i = 1, 2) indicate the preferential growth along [111]- orientation, confirming growth without any secondary phase. Furthermore, the BTO/STO SLs and BTO/STO-BFO SPE films exhibit (111) main peak (labeled as "0") accompanied by characteristic satellite peaks (labeled as ±1, ±2, ...), unambiguously verifying the formation of a periodic BTO/STO SLs. Notably, the BTO diffraction peak exhibits a small-angle shift following BFO incorporation, which we attribute to BFO-induced out-of-plane lattice expansion of the SLs to accommodate the compressive strain from the STO substrate[34]. This observation was further confirmed by RSM around the (222) reflection, as shown in Figure 2B-D. For the BTO film, the RSM pattern sequentially displays diffraction peaks from the STO substrate, SRO buffer layer, and BTO film from top to bottom in Figure 2B, confirming the highly epitaxial single-crystalline nature of the BTO film without any secondary phases or randomly oriented grains. After introducing STO, distinct satellite peaks emerged in the RSM image [Figure 2C] in addition to the STO, SRO, and BTO diffraction peaks (the absence of the SL(-2) reflection in Supplementary Figure 1 is attributed to its relatively weak intensity), further demonstrating the formation of a high-quality and regularly arranged SLs composed of BTO and STO. We observed upward and leftward shifts in the Q_Z and Q_X values of the main BTO diffraction peak respectively, indicating that the BTO layer in the superlattice is constrained by the STO layer, resulting in in-plane compressive strain and out-of-plane tensile strain. This is caused by the lattice mismatch between the STO layer (~3.905 Å) and the BTO layer (~3.992 Å). After the introduction of BFO to form the BTO/STO-BFO structure, the mutual dissolution of BTO and BFO weakened the diffraction intensity of the superlattice, leading to a reduction on

satellite peaks in Figure 2D. Additionally, the rightward shift of the main BTO diffraction peak in Q_X indicates that the strain state of the thin film transitioned to stronger in-plane compressive strain. This is because the incorporation of BFO reduced the overall average lattice constant and increased the lattice mismatch. Importantly, these results are consistent with the XRD observations, where the main BTO diffraction peak first shifted to higher angles with STO insertion and remained unchanged after BFO incorporation in Figure 2A. To further characterize the microstructure of the BTO/STO-BFO SPE film, we performed cross-STEM analysis [Figure 2E]. The STEM images reveal sharp interfaces between the STO substrate, SRO bottom electrode layer and BTO/STO-BFO functional layer. Among them, the thicknesses of the SRO and the BTO/STO-BFO layers are approximately 17 and 475 nm respectively, and each element is uniformly distributed without diffusion in the corresponding functional layer [Supplementary Figure 2]. Most significantly, the BTO/STO-BFO layer exhibits pronounced SLs ordering in the STEM image. To verify the compositional modulation of the SLs, we performed localized elemental analysis on a selected region of the BTO/STO-BFO layer [Figure 2F]. EDS mapping revealed the uniform distribution of Ba and Sr elements in the BTO and STO layers, with a thickness ratio of approximately 3:1. It is worth emphasizing that this thickness ratio was optimized and determined through systematic experimental studies in our previous work[18,20]. Moreover, line-scan analysis along the marked region (positions 1 → 2 in Figure 2F) demonstrates strict spatial confinement of Ba and Sr to their respective BTO and STO layers in Supplementary Figure 3, proving that the SLs is formed by the stacking of BTO and STO layers, corresponding to the previous XRD and RSM results. In addition, Bi and Fe elements are uniformly distributed in small amounts throughout the superlattice [Supplementary Figure 4]. The BTO/STO SLs and the solid solution of BFO are further examined by high-resolution STEM observations along the [110] axis in Figure 2G. The Ba and Sr elements successively occupied the A position in the crystal structure in EDS images, while the Ti element mainly occupied the B position, revealing atomically sharp interface with heteroepitaxial relationships of BTO[111]-STO[111]. Furthermore, the presence of Bi and Fe elements also demonstrates the successful solid-solution of BFO into the BTO/STO superlattice results. This was achieved by bombarding the BFO target in a multi-target rapid switching mode, and thus it is randomly and uniformly solid-solution distributed in the atoms. These comprehensive microstructural analyses confirm the successful fabrication of [111]-oriented BTO/STO-BFO SPE film with precisely controlled compositional modulation, wherein STO and BFO respectively exist in a layered structure and a solid solution form, fully consistent with our proposed design strategy in Figure 1.

To verify the energy storage performance of BTO/STO-BFO SPE film, the polarization-electric field (P-E) loops of BTO, BTO/STO SLs and BTO/STO-BFO SPE films are measured under the same electric field (E = 0.63 MV/cm), as shown in Figure 3A. Notably, Figure 3A was achieved by optimizing the growth parameters for STO and BFO [Supplementary Figures 5-7]. From the figure, the P-E loop of the BTO thin film capacitor exhibits a classic FE hysteresis, with P_s and P_r of 21.47 and 5.76 μC/cm², respectively. When the STO layer was introduced into BTO, the resulting BTO/STO SLs exhibited a slenderer loop shape with significantly suppressed hysteresis at room temperature[16]. After incorporating highly polarization BFO, the polarization of the BTO/STO-BFO SPE film exhibited a marked enhancement. Meanwhile, the current- electric field (I-E) curves of all thin films exhibit double switching peaks corresponding to FE hysteresis behavior, confirming its characteristic FE properties. Especially, the BTO/STO-BFO SPE film demonstrates lower current. Subsequently, we measured the P-E hysteresis loops of the films at their maximum E_{bre} in Figure 3B. Remarkably, through the combined strategy of STO layer insertion and BFO solid-solution incorporation, the BTO/STO-BFO film achieved a 330.48% improvement in E_{bre}, increasing from 1.05 to 3.47 MV/cm. Moreover, the hysteresis loop showed significant contraction by an approximately two-fold enhancement in P_s (increased from 25.29 to 46.52 μC/cm²), while the P_r decreased from 5.67 to 2.09 μC/cm². To further analyze the electric-field-driven electrical properties of the BTO/STO-BFO SPE film, we systematically measured P-E loops under varying E [Figure 3C]. We observed that the hysteresis loop gradually transitions

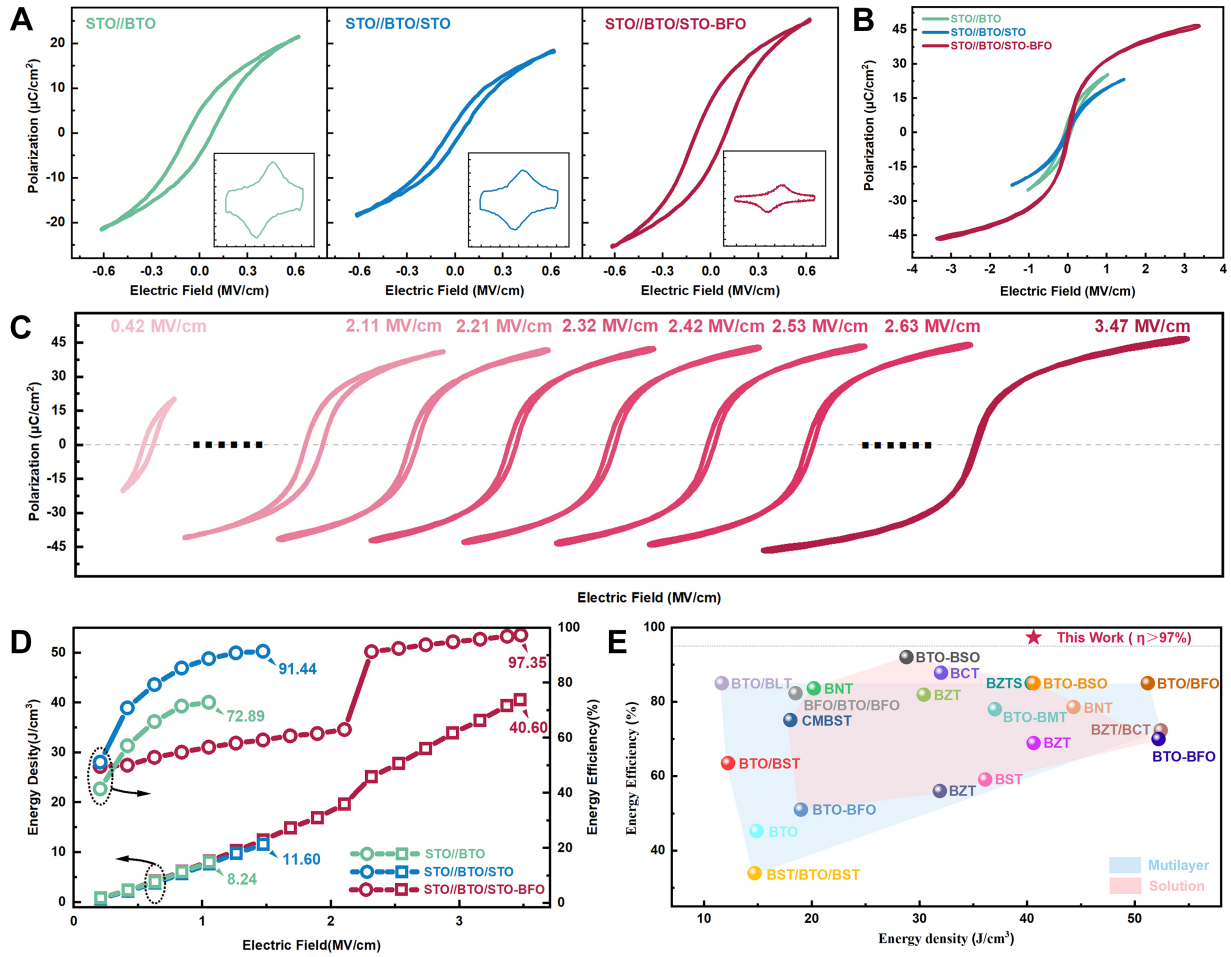

Figure 3. The energy storage performance of BTO/STO-BFO SPE film on (111)-STO substrate. (A) The P-E loops of BTO, BTO/STO SLs and BTO/STO-BFO SPE films under the same electric field, and the inset shows the corresponding I-E curves; (B) The P-E loops of BTO, BTO/STO SLs and BTO/STO-BFO SPE films under the E_{bre}; (C) The P-E loops of BTO/STO-BFO SPE film under different E; (D) The W_{rec} and η of BTO, BTO/STO SLs and BTO/STO-BFO SPE films with different E; (E) Comparison of W_{rec} and η with those reported in literatures. BTO: Barium titanate; STO: strontium titanate; BFO: bismuth ferrite; SLs: superlattices; SPE: superparaelectric; P-E: polarization-electric field; I-E: current-electric field; E: electric field; E_{bre}: electric breakdown strength; W_{rec}: recoverable energy density; η: energy storage efficiency; BNT: $Ba1-xNi_xTiO_3$; BZTS: $BaZr_{0.2}Ti_{0.8}O_3$-2%Sm_2O_3; BLF: $Bi_{0.993}La_{0.007}FeO_3$; CMBST: (Ce, Mn) co-doped $Ba_{0.6}Sr_{0.4}TiO_3$; BSO: $BiScO_3$; BMT: $Bi(Mg, Ti)O_3$; BZT: barium zirconate titanate; BCT: barium calcium titanate; BTO-BFO: barium titanate-bismuth ferrite; BST: barium strontium titanate; BTO-BST: barium titanate-barium strontium titanate.

from FE to RFE in low E, and eventually becomes a SPE state at high E, arising from the combined effects of the STO layer and BFO solid-solution. The field-dependent energy storage performance confirms our result [Figure 3D]. The BTO/STO-BFO SPE film exhibits FE behavior with a relatively low η below 2.11 MV/cm. When the E exceeds this critical threshold, η increases sharply as the film transitions to RFE. Ultimately at 3.47 MV/cm, the film achieves SPE while reaching both high W_{rec} (40.60 J/cm³) and exceptional η (97.35%), corresponding to 492.72% and 133.56% increases compared to pure BTO film. The key performance metrics of the BTO, BTO/STO and BTO/STO-BFO films are shown in Table 1.

This simultaneous enhancement of W_{rec} and η in BTO/STO-BFO SPE film originate from two aspects. On the one hand, the synergistic effect between periodic STO layers and BFO solid solution elevates the breakdown barrier and suppresses conductive path formation, thereby significantly improving E_{bre}. The other hand, the disrupted long-range ordering facilitates the transformation of nanodomains into highly polarized configurations, effectively increasing the ΔP[35,36]. Moreover, the well-maintained P-E loops among 25-150 °C

Table 1. Key performance metrics of the film capacitor

Film capacitor	E_{bre} (MV/cm)	P_s (μC/cm²)	P_r (μC/cm²)	W_{rec} (J/cm³)	η (%)
BTO	1.05	25.29	5.67	8.24	72.89
BTO/STO	1.47	23.33	2.37	11.60	91.44
BTO/STO-BFO	3.47	46.52	2.09	40.60	97.35

BTO: Barium titanate; STO: strontium titanate; BFO: bismuth ferrite; E_{bre}: electric breakdown strength; Ps: saturation polarization; Pr: remanent polarization; W_{rec}: recoverable energy density; η: energy storage efficiency.

in Supplementary Figure 8 suggests that the film can work at a broad temperature range. To highlight the advantages of our approach over individual engineering strategies, W_{rec} and η for BTO-based materials reported in literatures[31,37-57] are presented in Figure 3E, and our BTO/STO-BFO SPE film clearly stands out with orders of magnitude ultrahigh η, demonstrating exceptional potential for practical capacitor applications.

To extend our work toward broader applications, we extended the design strategy to flexible mica substrate and successfully fabricated flexible BTO/STO-BFO SPE film. Notably, an additional CFO buffer layer was introduced between the mica and the functional layers to address the significant structural mismatch and chemical incompatibility between mica and the FE films. As evidenced by the P-E loops with different E in Figure 4A, the flexible BTO/STO-BFO SPE film maintain polarization intensities comparable to those on STO substrate. Moreover, the local grey area reveals significant contraction of the hysteresis loop with increasing E, which is consistent with the P-E loops observed in films grown on STO substrates. More importantly, the transition from FE to RFE to SPE is a stable and reversible process [Supplementary Figure 9], which can be repeatedly achieved by alternating the application of low and high E_{bre}. Consequently, flexible BTO/STO-BFO SPE film still achieve impressive performance metrics of 34.37 J/cm³ and 97.48% at 2.74 MV/cm [Figure 4B], though the slightly inferior structural/thermal stability of mica substrate results in a reduced E_{bre}. The flexible BTO/STO-BFO SPE film demonstrated excellent energy storage stability under harsh environmental conditions, as verified through high-temperature, bending radius, and bending cycle experiments. Within the temperature range of 25 to 180 °C, the P-E loops, P_s and P_r remain nearly unchanged in Figure 4C and Supplementary Figure 10A. The W_{rec} and η have remained stable at 29.26 ± 1.04 J/cm³ and 96.86% ± 0.92% respectively, and its change rates are both less than 5% [Figure 4D], demonstrating the outstanding high-temperature stability of the flexible BTO/STO-BFO SPE film over a broad temperature range. Similarly, Figure 4E and Supplementary Figure 10B shows the excellent electrical stability in flexible BTO/STO-BFO SPE film under bending conditions (R = 10 to 4 mm). The energy storage performance reached its minimum at R = 6 mm, with W_{rec} and η of 28.56 J/cm³ and 95.51% respectively [Figure 4F]. We further conducted repeated bending tests [Figure 4G], and it is observed that the P_s, P_r and ΔP of P-E loops after 300, 400, 500 and 1,000 bending cycles are quite stable as well in Supplementary Figure 10C. Meanwhile, the energy storage performance remained robust, with W_{rec} and η consistently maintained around 29.03 J/cm³ and 96.20%, exhibiting minimal variations of only 1.62% and 0.73% [Figure 4H]. Additionally, SEM images and EDS of the film after 1,000 bending cycles [Supplementary Figures 11 and 12] confirmed that its microstructure remained intact with excellent homogeneity. These results demonstrate that the flexible BTO/STO-BFO SPE film simultaneously possess outstanding thermal stability and robust mechanical flexibility, exhibiting significant potential for flexible energy storage device applications.

CONCLUSIONS

In summary, we propose a multi-level synergistic modulation strategy combining interface engineering of the STO layer and entropy optimization via BFO solid-solution, achieved simultaneous enhancement of breakdown field strength and saturation polarization while effectively suppressing hysteresis loss, leading to

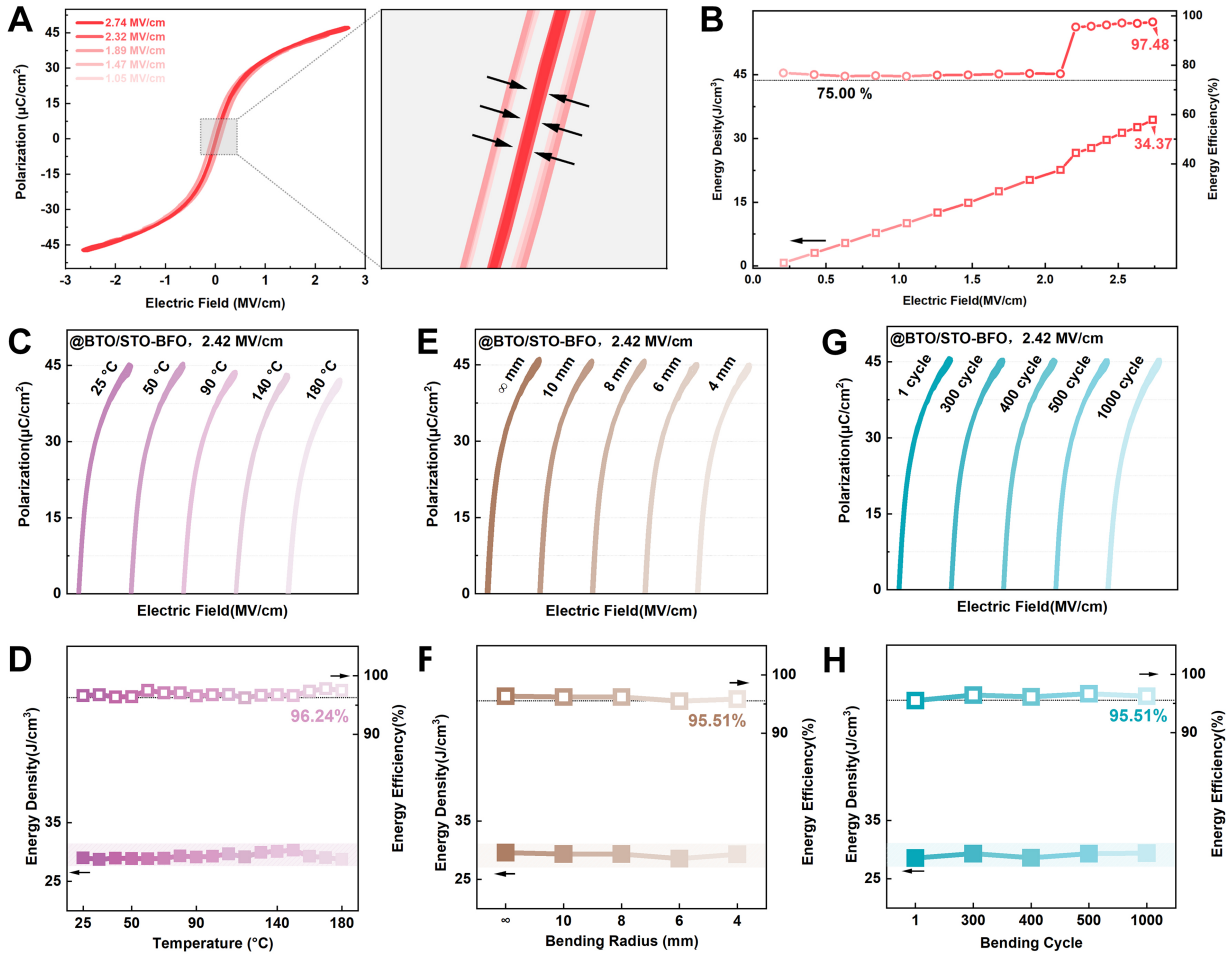

Figure 4. The energy storage performance of flexible BTO/STO-BFO SPE film on mica substrate. (A) The P-E loops of flexible BTO/STO-BFO SPE film under different E, and the local grey area have been magnified; (B) The W_{rec} and η of flexible BTO/STO-BFO SPE film with different E; (C-H) The P-E loops and energy storage performance of flexible BTO/STO-BFO SPE film under (C and D) different temperature, (E and F) bending radii and (G and H) bending cycle. BTO: Barium titanate; STO: strontium titanate; BFO: bismuth ferrite; SPE: superparaelectric; P-E: polarization-electric field; E: electric field; W_{rec}: recoverable energy density; η: energy storage efficiency.

dramatically improved energy storage performance. The optimized BTO/STO-BFO SPE film capacitors demonstrate an ultrahigh η of 97.35% and a remarkable W_{rec} of 40.60 J/cm³, representing 133.56% and 492.72% improvements respectively over pure BTO film. Furthermore, the flexible capacitors designed based on this strategy maintain excellent energy storage performance with high stability across wide temperature ranges and under various severe bending deformations, verifying the universality of our multi-level cooperative regulation strategy. This work provides a promising solution for the coordinated optimization of multiple parameters and comprehensive enhancement of energy storage performance in film capacitor.

DECLARATIONS

Authors' contributions

Conception and coordination of the project: Zhong, X. L.; Zhong, G.;
Sample fabrication: Chen, Q.; Su, P.;
Supervision of sample fabrication: Zhong, X.; Wang, J.; Li, J.; Zhong, G.;
Structure analysis and interpretation: Chen, Q.; Cheng, M.; Song, H.;
Writing the manuscript: Chen, Q.; Zhong, X.; Zhong, G.;
All authors participated in discussions and analysis.

Availability of data and materials

Some results of supporting the study are presented in the Supplementary Materials.

AI and AI-assisted tools statement

Not applicable.

Financial support and sponsorship

This work was supported by National Key Research and Development Program of China (2022YFF0706100 and 2024YFA1410600), National Natural Science Foundation of China (No. 62474186, 12275230 and 52472139), Shenzhen Science and Technology Program (JCYJ20240813155702004), Postgraduate Scientific Research Innovation Project of Hunan Province (No. CX20230654), and Project of Yuelushan Center for Industrial Innovation (Grant No. 2025YCII0224).

Conflicts of interest

Li, J. is a Senior Editorial Board Member of *Microstructures*. Li, J. was not involved in any steps of editorial processing, notably including reviewers' selection, manuscript handling, and decision making. The other authors declare that there are no conflicts of interest.

Ethical approval and consent to participate

Not applicable.

Consent for publication

Not applicable.

Supplementary Materials

Supplementary Materials

REFERENCES

1. Yang, C.; Lv, P.; Qian, J.; et al. Fatigue-free and bending-endurable flexible Mn-doped $Na_{0.5}Bi_{0.5}TiO_3$-$BaTiO_3$-$BiFeO_3$ film capacitor with an ultrahigh energy storage performance. *Adv. Energy. Mater.* **2019**, *9*, 1803949. DOI
2. Wang, K.; Ouyang, J.; Wuttig, M.; et al. Superparaelectric $(Ba_{0.95},Sr_{0.05})(Zr_{0.2},Ti_{0.8})O_3$ ultracapacitors. *Adv. Energy. Mater.* **2020**, *10*, 2001778. DOI
3. Yang, B.; Zhang, Y.; Pan, H.; et al. High-entropy enhanced capacitive energy storage. *Nat. Mater.* **2022**, *21*, 1074-80. DOI PubMed
4. Liu, Y.; Zhang, Y.; Wang, J.; et al. Ultrahigh capacitive energy storage through dendritic nanopolar design. *Science* **2025**, *388*, 211-6. DOI PubMed
5. Lu, R.; Wang, J.; Duan, T.; et al. Metadielectrics for high-temperature energy storage capacitors. *Nat. Commun.* **2024**, *15*, 6596. DOI PubMed PMC
6. Yu, Y.; Zhang, Q.; Xu, Z.; et al. Structure-evolution-designed amorphous oxides for dielectric energy storage. *Nat. Commun.* **2023**, *14*, 3031. DOI PubMed PMC
7. Pan, H.; Li, F.; Liu, Y.; et al. Ultrahigh-energy density lead-free dielectric films via polymorphic nanodomain design. *Science* **2019**, *365*, 578-82. DOI PubMed
8. Shu, L.; Shi, X.; Zhang, X.; et al. Partitioning polar-slush strategy in relaxors leads to large energy-storage capability. *Science* **2024**, *385*, 204-9. DOI PubMed
9. Ren, C.; Zhong, G.; Xiao, Q.; et al. Highly robust flexible ferroelectric field effect transistors operable at high temperature with low-power consumption. *Adv. Funct. Mater.* **2019**, *30*, 1906131. DOI
10. Sun, N.; Du, J.; Zhao, Y.; et al. Flexible multilayer lead-free film capacitor with high energy storage performances via heterostructure engineering. *J. Materiomics.* **2022**, *8*, 772-80. DOI
11. Zhang, S. High entropy design: a new pathway to promote the piezoelectricity and dielectric energy storage in perovskite oxides. *Microstructures* **2022**, *3*, 2023003. DOI PubMed
12. Jiang, M.; Peng, Z.; Zhou, Q.; et al. Superior energy storage performance of BNT-based ferroelectric ceramics based on maintaining high polarization and breakdown strength. *J. Adv. Dielect.* **2023**, *14*, 2340005. DOI
13. Kim, J.; Saremi, S.; Acharya, M.; et al. Ultrahigh capacitive energy density in ion-bombarded relaxor ferroelectric films. *Science* **2020**, *369*, 81-4. DOI PubMed

14. Pan, Z.; Wang, P.; Hou, X.; et al. Fatigue-free aurivillius phase ferroelectric thin films with ultrahigh energy storage performance. *Adv. Energy. Mater.* **2020**, *10*, 2001536. DOI
15. Feng, M.; Feng, Y.; Zhang, T.; et al. Recent advances in multilayer-structure dielectrics for energy storage application. *Adv. Sci.* **2021**, *8*, e2102221. DOI
16. Lupi, E.; Wexler, R. B.; Meyers, D.; et al. Engineering relaxor behavior in $(BaTiO_3)_n/(SrTiO_3)_n$ Superlattices. *Adv. Mater.* **2023**, *35*, e2302012. DOI PubMed
17. Zhang, X.; Shu, L.; Yang, Z.; et al. Ultra-thin multilayer films for enhanced energy storage performance. *Nano. Energy.* **2024**, *121*, 109271. DOI
18. Chen, Q.; Zhang, Y.; Tang, M.; et al. Significantly enhanced energy storage density and efficiency in flexible $Bi_{3.15}Nd_{0.85}Ti_3O_{12}$ thin film via periodic dielectric layers. *J. Appl. Phys.* **2022**, *131*, 114101. DOI
19. Zhang, A. H.; Wang, W.; Li, Q. J.; et al. Internal-strain release and remarkably enhanced energy storage performance in PLZT-$SrTiO_3$ multilayered films. *Appl. Phys. Lett.* **2020**, *117*, 252901. DOI
20. Zhong, G.; Chen, Q.; Zhang, Y.; et al. Van der Waals epitaxy enables rollable dielectric superlattice for record high overall energy density. *Adv. Funct. Mater.* **2023**, *33*, 2213752. DOI
21. Fan, X.; Wang, J.; Yuan, H.; Zheng, Z.; Zhang, J.; Zhu, K. Multi-scale synergic optimization strategy for dielectric energy storage ceramics. *J. Adv. Ceramics.* **2023**, *12*, 649-80. DOI
22. Zhang, L.; Pu, Y.; Chen, M.; Peng, X.; Wang, B.; Shang, J. Design strategies of perovskite energy-storage dielectrics for next-generation capacitors. *J. Eur. Ceram. Soc.* **2023**, *43*, 5713-47. DOI
23. Dai, S.; Li, M.; Wu, X.; et al. Combinatorial optimization of perovskite-based ferroelectric ceramics for energy storage applications. *J. Adv. Ceram.* **2024**, *13*, 877-910. DOI PubMed
24. Liu, X.; Zhu, J.; Li, Y.; Yang, T.; Hao, X.; Gong, W. High-performance PbZrO3-based antiferroelectric multilayer capacitors based on multiple enhancement strategy. *Chem. Eng. J.* **2022**, *446*, 136729. DOI
25. Ma, Z.; Li, Y.; Zhao, Y.; et al. High-performance energy-storage ferroelectric multilayer ceramic capacitors *via* nano-micro engineering. *J. Mater. Chem. A.* **2023**, *11*, 7184-92. DOI
26. Li, D.; Liu, Z.; Zhao, W.; et al. Global-optimized energy storage performance in multilayer ferroelectric ceramic capacitors. *Nat. Commun.* **2025**, *16*, 188. DOI PubMed PMC
27. Raza, H.; Cheng, J.; Lin, C.; Majumder, S.; Zheng, G.; Chen, G. High-entropy stabilized oxides derived via a low-temperature template route for high-performance lithium-sulfur batteries. *EcoMat* **2023**, *5*, e12324. DOI
28. Raza, H.; Cheng, J.; Wang, J.; Kandasamy, S.; Zheng, G.; Chen, G. Titanium-containing high entropy oxide (Ti-HEO): a redox expediting electrocatalyst towards lithium polysulfides for high performance Li-S batteries. *Nano. Research. Energy.* **2024**, *3*, e9120116. DOI PubMed
29. Raza, H.; Cheng, J.; Kandasamy, S.; et al. Manganese-ncorporated single-hase high-ntropy oxide modified separator enabled high performance of lithium-ulfur batteries at high sulfur loading. *Energy. Environ. Mater.* **2025**, *8*, e70058. DOI
30. Raza, H.; Cheng, J.; Xu, J.; et al. Harnessing high entropy sulfide (HES) as a robust electrocatalyst for long-erm cycling of lithium-ulfur batteries. *Energy. Environ. Mater.* **2025**, *8*, e70007. DOI
31. Chen, L.; Deng, S.; Liu, H.; Wu, J.; Qi, H.; Chen, J. Giant energy-storage density with ultrahigh efficiency in lead-free relaxors via high-entropy design. *Nat. Commun.* **2022**, *13*, 3089. DOI PubMed PMC
32. Duan, J.; Wei, K.; Du, Q.; et al. High-entropy superparaelectrics with locally diverse ferroic distortion for high-capacitive energy storage. *Nat. Commun.* **2024**, *15*, 6754. DOI PubMed PMC
33. Zhou, Y.; Zhang, T.; Chen, L.; et al. Design of antiferroelectric polarization configuration for ultrahigh capacitive energy storage via increasing entropy. *Nat. Commun.* **2025**, *16*, 805. DOI PubMed PMC
34. Cho, S.; Yun, C.; Kim, Y. S.; et al. Strongly enhanced dielectric and energy storage properties in lead-free perovskite titanate thin films by alloying. *Nano. Energy.* **2018**, *45*, 398-406. DOI
35. Liu, Y.; Yang, B.; Lan, S.; Pan, H.; Nan, C.; Lin, Y. Perspectives on domain engineering for dielectric energy storage thin films. *Appl. Phys. Lett.* **2022**, *120*, 150501. DOI
36. Liu, Y.; Liu, J.; Pan, H.; et al. Phase-field simulations of tunable polar topologies in lead-free ferroelectric/paraelectric multilayers with ultrahigh energy-storage performance. *Adv. Mater.* **2022**, *34*, e2108772. DOI PubMed
37. Diao, C.; Liu, H.; Zheng, H.; et al. Enhanced energy storage properties of $BaTiO_3$ thin films by $Ba_{0.4}Sr_{0.6}TiO_3$ layers modulation. *J. Alloys. Compd.* **2018**, *765*, 362-8. DOI
38. Fu, D.; He, F.; Tian, H.; et al. Ni-modified $BaTiO_3$ film prepared by sol-gel with high energy storage performance. *Ceram. Int.* **2024**, *50*, 52004-10. DOI
39. Abbas, W.; Ho, D.; Pramanick, A. High energy storage efficiency and thermal stability of A-site-deficient and 110-textured $BaTiO_3$-iScO_3 thin films. *J. Am. Ceram. Soc.* **2020**, *103*, 3168-77. DOI

40. Hou, Y.; Han, R.; Li, W.; Luo, L.; Fei, W. Significantly enhanced energy storage performance in $BiFeO_3/BaTiO_3/BiFeO_3$ sandwich-structured films through crystallinity regulation. *Phys. Chem. Chem. Phys.* **2018**, *20*, 21917-24. DOI
41. Zhang, M.; Deng, C. Structure, ferroelectric and energy density properties of $BaTiO_3$ film capacitors for energy storage applications. *Mod. Phys. Lett. B.* **2021**, *35*, 2150179. DOI
42. Hu, Y.; Xie, Q.; Liang, R.; et al. High energy storage performance in lead-free BiFeO3-BaTiO3 ferroelectric thin film fabricated by pulsed laser deposition. *AIP. Advances.* **2019**, *9*, 085005. DOI
43. Zhu, H.; Liu, M.; Zhang, Y.; Yu, Z.; Ouyang, J.; Pan, W. Increasing energy storage capabilities of space-charge dominated ferroelectric thin films using interlayer coupling. *Acta. Mater.* **2017**, *122*, 252-8. DOI
44. Sun, Z.; Tian, X.; Shang, L.; et al. Modifying energy storage performances of new lead-free system ferroelectric capacitors through interfacial stress. *Appl. Surf. Sci.* **2021**, *559*, 149992. DOI
45. Instan, A. A.; Mishra, K. K.; Katiyar, R. S. Ferroelectric ordering and energy storage capacity in lead-free $Ba(Zr_{0.2}Ti_{0.8})O_3$ nanoscale film capacitors fabricated using pulsed laser deposition technique. *J. Appl. Phys.* **2019**, *126*, 134101. DOI
46. Sun, Z.; Ma, C.; Wang, X.; et al. Large energy density, excellent thermal stability, and high cycling endurance of lead-free $BaZr_{0.2}Ti_{0.8}O_3$ film capacitors. *ACS. Appl. Mater. Interfaces.* **2017**, *9*, 17096-101. DOI PubMed
47. Sun, Z.; Ma, C.; Liu, M.; et al. Ultrahigh energy storage performance of lead-free oxide multilayer film capacitors via interface engineering. *Adv. Mater.* **2017**, *29*, 1604427. DOI PubMed
48. Puli, V. S.; Pradhan, D. K.; Adireddy, S.; et al. Nanoscale polarisation switching and leakage currents in $(Ba_{0.955}Ca_{0.045})(Zr_{0.17}Ti_{0.83})O_3$ epitaxial thin films. *J. Phys. D. Appl. Phys.* **2015**, *48*, 355502. DOI
49. Zhu, X.; Guo, M.; Sun, B.; et al. Significantly enhanced energy storage density of epitaxial $Ba_{0.53}Sr_{0.47}TiO_3$ thin films by optimizing bottom electrode material. *Ceram. Int.* **2020**, *46*, 13900-6. DOI
50. Ortega, N.; Kumar, A.; Scott, J. F.; et al. Relaxor-ferroelectric superlattices: high energy density capacitors. *J. Phys. Condens. Matter.* **2012**, *24*, 445901. DOI PubMed
51. Qian, J.; Yang, C.; Han, Y.; Sun, X.; Chen, L. Reduced leakage current, enhanced energy storage and dielectric properties in (Ce,Mn)-codoped $Ba_{0.6}Sr_{0.4}TiO_3$ thin film. *Ceram. Int.* **2018**, *44*, 20808-13. DOI
52. Kwon, D. K.; Lee, M. H. Temperature-stable high-energy-density capacitors using complex perovskite thin films. *IEEE. Trans. Ultrason. Ferroelectr. Freq. Control.* **2012**, *59*, 1894-9. DOI PubMed
53. Ren, L.; Guo, K.; Cui, R.; et al. High energy storage performance in BTO-based ferroelectric films. *Ceram. Int.* **2024**, *50*, 41931-42. DOI
54. Liang, Z.; Liu, M.; Shen, L.; et al. All-inorganic flexible embedded thin-film capacitors for dielectric energy storage with high performance. *ACS. Appl. Mater. Interfaces.* **2019**, *11*, 5247-55. DOI PubMed
55. Zhao, T.; Ye, Y.; Guo, K.; et al. High energy storage properties of calcium-doped barium titanate thin films with high breakdown field strength. *J. Alloys. Compd.* **2024**, *970*, 172487. DOI
56. Balmuchu, S. P.; Sahu, S.; Dobbidi, P. The effect of interfacial charge-induced multiferroic properties of $Bi_{0.993}La_{0.007}FeO_3/BaTiO_3$ bilayer thin films: performance modulation and energy storage applications. *Surf. Interfaces.* **2024**, *44*, 103653. DOI
57. Abbas, W.; Ho, D.; Pramanick, A. High energy efficiency and thermal stability of $BaTiO_3$-$BiScO_3$ thin films based on defects engineering. *ACS. Appl. Electron. Mater.* **2021**, *3*, 1097-106. DOI